

This section contains shorter technical papers. These shorter papers will be subjected to the same review process as that for full papers.

Numerical Solutions of Turbulent Convection Over a Flat Plate With Angle of Attack

N. T. Truncellito,^{1,2} H. Yeh,^{1,3} and N. Lior^{1,3}

Nomenclature

- A = constant used in initial data line for the turbulent kinetic energy, equation (14)
 A_q = turbulent empirical constant = 0.22, equation (3)
 A^+ = effective sublayer thickness, in equation (9)
 B = exponential constant used in turbulent kinetic energy distribution initial data line = 1, equation (14)
 B_q = turbulent empirical constant = 0.38, equation (7)
 c_f = skin friction coefficient = $(\mu \Delta \bar{u} / \Delta y)_w / \frac{1}{2} \rho U_\infty^2$
 c_p = specific heat at constant pressure
 D = Van Driest damping function, equation (9)
 g_x = component of gravitational constant in x direction
 k = thermal conductivity
 l = Prandtl mixing length
 L = length of flat plate
 Nu_x = local Nusselt number = $(-k \Delta \bar{T} / \Delta y)_w x / [k (T_w - T_\infty)]$
 p = pressure
 Pr = Prandtl number
 Pr_t = turbulent Prandtl number = 0.85
 $q^2/2$ = turbulent kinetic energy/fluid density
 Re = Reynolds number
 Re_L = local Reynolds number based on L
 Re_{ref} = $\rho_{ref} L_{ref} U_{ref} / \mu_{ref}$
 Re_x = local Reynolds number based on x

- S_{cq} = turbulent empirical constant = 1.7, equation (7)
 T = temperature
 \bar{u} = mean velocity component in streamwise x direction
 U = free-stream velocity
 u' = fluctuating velocity component in x direction
 v = total velocity in y direction, including mean and fluctuating components
 \bar{v} = mean velocity
 v' = fluctuating velocity component in y direction
 x = coordinate along plate in streamwise direction
 X = body force, e.g., buoyancy
 y = coordinate measured normal to plate
 y^+ = normalized y coordinate, equation (10)
 γ = ratio of specific heats = c_p / c_v
 $\Delta \xi$ = x/L
 δ = boundary layer thickness
 θ = flat-plate angle of attack with respect to the free stream, deg
 κ = empirical constant in turbulent flow = 0.41, equation (3)
 μ = dynamic viscosity
 ν = kinematic viscosity
 ξ = Patankar-Spalding coordinate in direction of flow = x/L
 ρ = density of fluid
 τ = shear stress
 ψ = stream function
 ω = Patankar-Spalding coordinate of local stream function ψ normalized by ψ_e at a specific location ξ

Subscripts

- e = conditions at the boundary layer edge (boundary with free stream)
 ref = reference conditions
 t = turbulent component
 w = wall conditions
 $wake$ = turbulent wake conditions
 x = local value measured at x
 ∞ = free-stream conditions

Superscripts

- $-$ = time-averaged value

¹Department of Mechanical Engineering and Applied Mechanics, University of Pennsylvania, Philadelphia, PA 19104.

²Systems Engineer, General Electric Co., Advanced Energy Programs Dept., Valley Forge, PA.

³Mem. ASME.

Contributed by the Heat Transfer Division for publication in the JOURNAL OF HEAT TRANSFER. Manuscript received by the Heat Transfer Division August 10, 1983.

1 Introduction

As evident from the literature [1–10], the knowledge of turbulent convection over flat plates with an angle of attack is limited principally to empirical results of overall heat transfer coefficients (possibly in the form of Nusselt numbers or Colburn j factors) in some ranges of the Reynolds number. This study was motivated in part by the lack of a conclusive method to determine heat loss due to wind effects on the exterior of inclined solar collectors and photovoltaic panels, as also evident from the widespread use of the Jurges correlation (reported in [4, 11]), which does not incorporate any dimensions or fluid properties and is thus strictly correct only for the size of plate and thermal conditions of Jurges' experiment. The purpose of this investigation is to examine the turbulent boundary layer flow and corresponding skin friction and convection heat loss as a function of free-stream velocity and angle of attack, by using a combined analytical/numerical approach. Many such approaches exist for the computation of turbulent flow [12–21]. The approach taken in this study was to establish and solve two models, a zeroth-order one and a first-order one, determine their validity by comparison to existing experimental results and correlations, and compare the effort required for their solution. Since it is generally accepted that the zero-order model is a reasonable approximation, it serves here as a base with which the first-order model solution accuracy and effort are compared. The most salient elements of the analysis and results are summarized below. More details can be found in [22].

2 Analysis

Briefly described, the continuity, momentum, and energy equations for a two-dimensional, turbulent, steady, time-averaged compressible boundary-layer flow over a plate with arbitrary angle of attack, and including a natural convection term, are transformed to the Patankar–Spalding [14] coordinate system. The eddy viscosity is formulated in terms of a three-region mixing length Prandtl–Von Karman model which incorporated the Van-Driest damping function in the near-wall viscous sublayer region.

In the zero-order model, which uses only the partial differential equations for the mean velocity field, and no turbulence partial differential equations (i.e., this is the usual algebraic mixing length model), the turbulent viscosity μ_t is expressed as

$$\mu_t = \bar{\rho} l^2 \left| \frac{\partial \bar{u}}{\partial y} \right| \quad (1)$$

where l is the Prandtl mixing length, and similarly the turbulent thermal conductivity

$$k_t = \bar{\rho} l^2 c_p \left| \frac{\partial \bar{u}}{\partial y} \right| / \text{Pr}_t \quad (2)$$

In the first-order model the turbulent viscosity is given as [13]

$$\mu_t = \rho (A_q l / \kappa) \sqrt{q^2 / 2} \quad (3)$$

where $q^2 = (\bar{u}'^2 + \bar{v}'^2)$. Similarly, the turbulent conductivity is

$$k_t = \mu_t c_p / \text{Pr}_t \quad (4)$$

Pr_t was assumed to be constant. Any variations in its value in the problem considered here would most likely produce only second-order effects.

The zeroth-order model is the usual algebraic mixing length model and the equations would therefore not be reproduced here. The equations for the first-order model are

Momentum:

$$\bar{\rho} \bar{u} \frac{\partial \bar{u}}{\partial \xi} + \bar{\rho} \bar{u} (\omega \rho_e v_e / \psi_e) \frac{\partial \bar{u}}{\partial \omega}$$

$$= -\frac{d\bar{p}}{d\xi} + (\bar{\rho} \bar{u} / \psi_e) \left\{ \left[\frac{\partial \mu}{\partial \omega} (1 / \text{Re}_{\text{ref}}) + \frac{\partial \rho}{\partial \omega} (A_q l / \kappa) \sqrt{q^2 / 2} + (\bar{\rho} A_q / \kappa) \frac{\partial l}{\partial \omega} \sqrt{q^2 / 2} + (A_q \bar{\rho} l / \kappa) \frac{\partial \sqrt{q^2 / 2}}{\partial \omega} \right] (\bar{\rho} \bar{u} / \psi_e) \frac{\partial \bar{u}}{\partial \omega} + [(\mu / \text{Re}_{\text{ref}}) + (A_q \bar{\rho} l / \kappa) \sqrt{q^2 / 2}] \left[\frac{\partial \bar{\rho}}{\partial \omega} (\bar{u} / \psi_e) \frac{\partial \bar{u}}{\partial \omega} + (\bar{\rho} / \psi_e) \left(\frac{\partial \bar{u}}{\partial \omega} \right)^2 + (\bar{\rho} \bar{u} / \psi_e) \frac{\partial^2 \bar{u}}{\partial \omega^2} \right] \right\} + X \quad (5)$$

where X is the buoyancy force defined as $g_x (\bar{T} - T_\infty) / T_\infty$.

Energy:

$$\bar{\rho} \bar{u} \frac{\partial \bar{T}}{\partial \xi} + \bar{\rho} \bar{u} (\omega / \psi_e) \bar{\rho}_e v_e \frac{\partial \bar{T}}{\partial \omega} = (\bar{\rho} \bar{u} / \psi_e) \frac{\partial}{\partial \omega} \left\{ [(\kappa / c_p) (\rho UL)_{\text{ref}}] + (A_q l / \kappa) \sqrt{q^2 / 2} (\bar{\rho} / \text{Pr}_t) (\bar{\rho} \bar{u} / \psi_e) \frac{\partial \bar{T}}{\partial \omega} \right\} + [(\mu / \text{Re}_{\text{ref}}) + (\bar{\rho} A_q l / \kappa) \sqrt{q^2 / 2}] \left[(\bar{\rho} \bar{u} / \psi_e) \frac{\partial \bar{u}}{\partial \omega} \right]^2 (u_{\text{ref}}^2 / c_p T_{\text{ref}}) + \bar{u} \frac{d\bar{p}}{d\xi} [(\gamma - 1) / \gamma] \quad (6)$$

Turbulent Energy [12, 13]:

$$\bar{\rho} \bar{u} \left[\frac{\partial (q^2 / 2)}{\partial \xi} + (\omega / \psi_e) \bar{\rho}_e v_e \frac{\partial (q^2 / 2)}{\partial \omega} \right] = \bar{\rho} (A_q / \kappa) l \sqrt{q^2 / 2} \left[(\bar{\rho} \bar{u} / \psi_e) \frac{\partial \bar{u}}{\partial \omega} \right]^2 - (\rho B_q \kappa / l) (q^2 / 2)^{3/2} + (\bar{\rho}^2 \bar{u} / \psi_e) \left\{ \left[(1 / \text{Re}_{\text{ref}}) \frac{\partial \nu}{\partial \omega} + (A_q / \kappa S c_q) \left(\frac{\partial l}{\partial \omega} \sqrt{q^2 / 2} + l \frac{\partial \sqrt{q^2 / 2}}{\partial \omega} \right) \right] \cdot (\bar{\rho} \bar{u} / \psi_e) \frac{\partial (q^2 / 2)}{\partial \omega} + [(\nu / \text{Re}_{\text{ref}}) + (A_q l / \kappa) (\sqrt{q^2 / 2} / S c_q) \left[\frac{\partial \bar{\rho}}{\partial \omega} (\bar{u} / \psi_e) \frac{\partial (q^2 / 2)}{\partial \omega} + (\bar{\rho} / \psi_e) \frac{\partial \bar{u}}{\partial \omega} \frac{\partial (q^2 / 2)}{\partial \omega} + (\bar{\rho} \bar{u} / \psi_e) \frac{\partial^2 (q^2 / 2)}{\partial \omega^2} \right] \right\} \quad (7)$$

The mixing length l is defined for three boundary layer regions.

In the viscous sublayer

$$l = \kappa y D \quad (8)$$

where D is the Van Driest damping function

$$D = 1 - \exp(-y^+ / A^+) \quad (9)$$

y^+ is the normalized y coordinate

$$y^+ = y (\sqrt{\tau_w / \rho_w}) / \nu_w \quad (10)$$

and A^+ is the effective sublayer thickness which was found to be approximately 26 based on experimental results in [13].

In the near wall regions, $26 < y^+ < y_{\text{wake}}^+$

$$l = \kappa y \quad (11)$$

where $\kappa = 0.41$.

In the wake region, defined by $y > 0.2\delta$, as suggested in [13]

$$l = 0.085\delta \quad (12)$$

The pressure gradient $dp/d\xi$ is supplied by the potential flow relation for an infinite wedge [3]. The ideal gas state equation was used, and the Sutherland model for the molecular viscosity [3], and constant thermal conductivity and specific heat were assumed. The coefficients used in the turbulent models are defined in the Nomenclature. The boundary conditions on the turbulent kinetic energy are that $q^2/2$ is zero at the wall and approaches free stream turbulence as $y \rightarrow \infty$

$$\lim_{y \rightarrow \infty} = 1.5(\overline{u'^2}) \quad (13)$$

where, based on results from wind-tunnel experiments, it was assumed that $\overline{u'^2}/U_\infty = 0.01$. An initial data line for the boundary condition was provided, and the following distribution was prescribed based upon results reported in [23]

$$q^2/2 = Aye^{-By^2} \quad (14)$$

where it was assumed that $B = 1$, and A was calculated from equations (13) and (14). For both models the boundary conditions at the plate are no-slip for the velocity, and arbitrarily specified temperature.

At the boundary layer edge, the initial guess for the stream function ψ_e , and the normal mass flow $(\rho v)_e$, needed in equations (5)–(7), are obtained from an integral solution of the turbulent boundary-layer momentum and energy equations for this wedge flow problem. The solution of the integrated equations is obtained by a fourth-order Runge-Kutta method which only took about 1 percent of the total computation time. The integral solution insured that a good upper limit to the boundary layer thicknesses was predicted initially, thus placing the numerical models' velocity and temperature profiles in the proper domain. This produced solutions with only a small number of iterations, or occasionally with none at all. U_e is obtained from the potential flow solution for the wedge [3].

3 Method of Solution

The momentum, energy, and turbulent kinetic energy equations (such as equations (5)–(7)) in the first-order model are placed in a linearized central finite difference form compatible with a tridiagonal matrix inversion solution scheme, implicit in the ω direction and explicit in the ξ direction.

The conditions required for the stability of the explicit part of this numerical scheme were evaluated to be

$$\Delta\xi \leq (\Delta\omega)^2 \quad (15)$$

The discretization error for the finite difference equations in both models is $O[(\Delta\omega)^2]$. For the zeroth-order model, well-behaved results were obtained for $\Delta\xi \leq 0.005$. A further reduction of 50 percent in $\Delta\xi$, to 0.0025, has changed Nu_x by only 4 percent. In comparison, the first-order solution scheme was significantly more sensitive, requiring $\Delta\xi$ steps which were smaller by a factor of about a thousand.

The present technique differs from existing procedures such as that described in [13] in that there is no need for a "match-up" or "join-point" near the wall. In [13], such a point is employed between the second and third nodes (normal to the wall) to join the near-wall (Couette layer) solution with that for the outer region (between the edges of the laminar sublayer and the overall turbulent boundary layer). In the present analysis, a finer mesh is employed near the wall (for example, five-fold finer in the zeroth-order model) to account adequately for the steep velocity and temperature gradients.

The velocity and temperature profiles obtained from both models were well-behaved distributions. More importantly, the turbulent kinetic energy profile was generated numerically and also shown to be well behaved.

4 Results

The Range of Variables. Results were obtained for Reynolds numbers up to about 3×10^5 , and angles of attack $\theta = 0, 30, 45$, and 60 deg. A constant air temperature of 20°C was assumed. Both models allow the specification of an arbitrary wall temperature, and unless indicated otherwise, a constant wall temperature of 100°F (37.8°C) was assumed in the cases shown below.

Zeroth-Order Model Results. For $\theta = 0$ deg, very good agreement was observed with the Eckert and Colburn equations (shown in [3]). The results were found to agree with the Jürges values only for $L = 2$ ft (0.61 m), and over a normalized velocity of 0–20. This is due to the fact that Jürges conducted his tests at these specific conditions. Substantial disagreement with the Jürges correlation was found for other plate lengths and velocities. The results were found to be consistent with the experimental data reported in the ASHRAE handbook [24] and with the JPL test data of [25] (the comparisons are presented in [22]).

Comparisons of the zeroth-order model results with the more recent measurements of Sparrow and Tien [1] for plates at different angles to the stream (performed by mass transfer experiments as an analog to heat transfer) indicate [22] that the zeroth-order results show a moderate effect of angle of attack between 30–60 deg with regard to wall heat transfer, while the data of [1] show no such effect. In general, it was found that in comparison with the first-order model, the zeroth-order model overpredicts the friction coefficient by about 6–35 percent and the Nusselt number by about 5–17 percent in the analyzed range of parameters.

The finite difference model results were also shown to compare well with the experimental data of Scesa and Sauer [6] obtained for a step discontinuity in wall temperature (see [22]).

First-Order Model Results. The first-order model results have been used to develop a correlation

$$c_{fx} = \left(\sum_{i=0}^3 a_{1i}\theta^i \right) \text{Re}^{-\left(\sum_{i=0}^3 b_{1i}\theta^i \right)} \quad (16)$$

and

$$\text{Nu}_x = \left(\sum_{i=0}^3 c_{1i}\theta^i \right) \text{Re}^{\left(\sum_{i=0}^3 d_{1i}\theta^i \right)} \text{Pr}^{1/3} \quad (17)$$

where θ is in degrees, valid for $0 \text{ deg} \leq \theta \leq 60 \text{ deg}$, and the coefficients a_{1i} , b_{1i} , c_{1i} , and d_{1i} are shown in Table 1. Here $\text{Re}_{\text{ref}} = 6240$, evaluated for $\rho_{\text{ref}} = 0.00234 \text{ lbf}\cdot\text{s}^2/\text{ft}^4$, $U_{\text{ref}} = 1 \text{ ft/s}$, $L_{\text{ref}} = 1 \text{ ft}$, and $\mu_{\text{ref}} = (3.75) 10^{-7} \text{ lbf}\cdot\text{s}/\text{ft}^2$.

Figures 1 and 2 show that the results of the first-order turbulence model for c_{fx} and Nu_x agree better, respectively, with the empirical Eckert and Colburn equations than the results of the zeroth-order model. In addition to the fact that the additional equation in the first-order model creates a stronger coupling between the constitutive relations, a much finer computational mesh had to be used in the first-order model (as

Table 1 Coefficients for equations (18) and (19)

Model	i =	0	1	2	3
First-Order	a_{1i}	$(5.00)10^{-2}$	$(2.63)10^{-3}$	$-(3.89)10^{-5}$	$(2.22)10^{-7}$
	b_{1i}	$(2.00)10^{-1}$	$(2.32)10^{-3}$	$-(5.83)10^{-5}$	$(4.81)10^{-7}$
	c_{1i}	$(2.90)10^{-2}$	$(3.09)10^{-3}$	$-(8.83)10^{-5}$	$(9.51)10^{-7}$
	d_{1i}	$(8.00)10^{-1}$	$-(5.01)10^{-3}$	$(1.36)10^{-4}$	$-(1.28)10^{-6}$

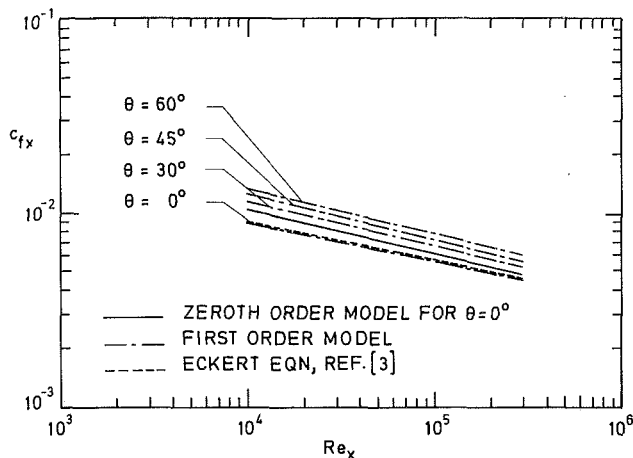


Fig. 1 Skin friction coefficient versus Reynolds number results obtained from first-order model

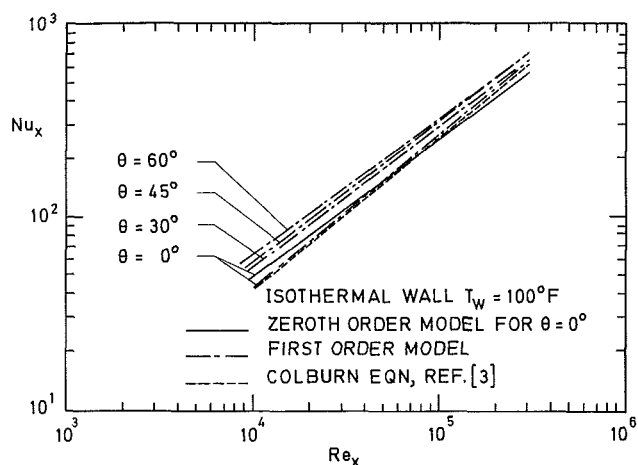


Fig. 2 Nusselt number versus Reynolds number results obtained from first-order model

described above), and this would produce a solution closer to reality, as indeed observed.

The natural convection effects on Nu were found to be negligible in the range of these calculations. This was to be expected, since the Grashof number in the cases computed is smaller than $0.225 Re^2$, indicating according to [27] that the effect of natural convection upon the average heat transfer coefficient should be less than 5 percent.

In attempting to apply the results of this two-dimensional analysis to heat transfer from real objects, such as solar collectors, in the natural environment (wind), one must note that most real objects introduce appreciable three-dimensional effects, as well as separation along the edges, and that the nature and level of free-stream turbulence have an important effect on flow characteristics and heat transfer [8-10]. With that in mind, it is obvious that the results obtained in this study must be applied with great care, to cases where the geometry and free-stream turbulence are similar. Although the existence of appreciable three-dimensional effects would require the solution of a different model, this model could be used with realistic values of the free-stream turbulence to give acceptable results for cases which allow a two-dimensional approximation (such as large surfaces, faired or baffled edges). The remarkable coincidence between these results and the empirical Eckert and Colburn correlations at zero angle of attack (the only angle for which these correlations were developed), are noteworthy.

5 Conclusions

- 1 An integral solution, which is relatively easy to obtain, provides good data for starting the numerical solution.
- 2 Cost-effective zeroth-order and first-order numerical solutions have been developed whereby any matching procedure between the laminar (Couette) sublayer and the outer turbulent mixing layer solutions has been eliminated.
- 3 The models were proven to be effective in predicting local Nusselt numbers for arbitrary wall temperature distributions.
- 4 The zeroth-order results agree very well, within 10-15 percent, with the Colburn and Eckert equations (for zero angle of attack) as well as several other sources (for nonzero angles) of measured skin friction and heat transfer data, while the first-order model results came even closer, within 1-2 percent. The first-order numerical model required, however, a grid which is about a thousand times finer than that needed for the zeroth-order model, and was much more sensitive to assumed starting profiles. This, of course, increased computation difficulty and time significantly.

Acknowledgments

This study was partially supported by the U.S. Department of Energy, Office of Conservation and Solar Applications, Solar Heating and Cooling R&D Branch. The senior author wishes to express his gratitude to Mr. William Auxer of the General Electric Co. for his encouragement of this research effort, and to Drs. I. M. Cohen and P. S. Ayyaswamy for their constructive comments.

References

- 1 Sparrow, E. M., and Tien, K. K., "Local Heat Transfer and Fluid Flow Characteristics for Airflow Oblique or Normal to a Square Plate," *Int. J. Heat and Mass Transfer*, Vol. 22, 1979, pp. 349-360.
- 2 Drake, R. M., "Investigation of the Variation of Point Unit Heat Transfer Coefficients for Laminar Flow Over an Inclined Flat Plate," *ASME J. Appl. Mech.*, Vol. 71, 1949, pp. 1-8.
- 3 Schlichting, H., *Boundary Layer Theory*, 6th ed., McGraw-Hill, New York, 1968.
- 4 McAdams, W. H., *Heat Transmission*, 3rd ed., McGraw-Hill, New York, 1954.
- 5 Avezov, R. R., and Vakhidov, A. T., "Choice of Controlling Dimension in the Oblique Flow Past the Glass Surface of a Solar Installation," *Applied Solar Energy*, Vol. 9, 1973, pp. 90-91.
- 6 Avezov, R. R., Akhmedaliev, A., and Kakhkharov, N. A., "Effect of Angle of Attack on the Efficiency and Heat Transfer of the Glass Cover of a Solar Installation Under Laminar-Flow Conditions," *Applied Solar Energy*, Vol. 9, 1973, pp. 45-48.
- 7 Hewitt, H. C., Jr., and Onur, N., "A Study of Wind Effects on Collector Performance," ASME Paper No. 80-C2/Sol-4, 1980.
- 8 Test, F. L., and Lessman, R. C., "An Experimental Study of Heat Transfer During Forced Convection Over a Rectangular Body," *ASME JOURNAL OF HEAT TRANSFER*, Vol. 102, 1980, pp. 146-151.
- 9 Test, F. L., Lessman, R. C., and Johari, A., "Heat Transfer During Wind Flow Over Rectangular Bodies in the Natural Environment," *ASME JOURNAL OF HEAT TRANSFER*, Vol. 103, 1981, pp. 262-267.
- 10 McCormick, D. C., Test, F. L., and Lessman, R. C., "The Effect of Free-Stream Turbulence on Heat Transfer From a Rectangular Prism," *ASME JOURNAL OF HEAT TRANSFER*, Vol. 106, 1984, pp. 268-275.
- 11 Duffie, J. A., and Beckman, W. A., *Solar Engineering of Thermal Processes*, Wiley-Interscience, New York, 1980.
- 12 Reynolds, W. C., "Computation of Turbulent Flows," *Annual Review of Fluid Mechanics*, Vol. 7, 1975, pp. 183-208.
- 13 Crawford, M. E., and Kays, W. M., "STAN-5—A Program for Numerical Computation of Two-Dimensional Internal/External Boundary Layer Flows," *Stanford University, Dept. of Mechanical Engineering, Report No. HMT-23*, 1975.
- 14 Patankar, S. V., and Spalding, D. B., *Heat and Mass Transfer in Boundary Layers*, 2nd ed., Intertext Books, London, 1970.
- 15 Launder, B. E., and Spalding, D. B., *Lectures in Mathematical Models of Turbulence*, Academic Press, London-New York, 1972.
- 16 Bradshaw, P., "The Understanding and Prediction of Turbulent Flow," *Aeronaut. J.*, Vol. 76, 1972, pp. 403-418.
- 17 Mellor, G. L., and Herring, H. L., "A Survey of the Mean Turbulent Field Closure Methods," *AIJA Journal*, Vol. 11, 1973, pp. 590-599.
- 18 Cebeci, T., et al., "Calculation of Three-Dimensional Compressible Boundary Layers on Arbitrary Wings," *Proc. NASA-Langley Conf. Aerodyn. Anal. Requiring Adv. Computers*, 1975.

- 19 Lumley, J. L., "Computational Modeling of Turbulent Flows," in: *Advances in Applied Mechanics*, Vol. 18, C.-S. Yih, ed., 1978, pp. 123-176.
- 20 Bradshaw, P., Cebeci, T., and Whitelaw, J. M., *Engineering Calculation Methods for Turbulent Flow*, Academic Press, New York, 1981.
- 21 Taylor, C., and Morgan, K., eds., *Computational Techniques in Transient and Turbulent Flow*, Pineridge Press, New York, 1981.
- 22 Truncellito, N. T., "Numerical Solutions of Turbulent Models for Flow Over a Plate With Angle of Attack," Ph.D. dissertation, Department of Mechanical Engineering and Applied Mechanics, University of Pennsylvania, Philadelphia, PA, 1981.
- 23 Hinze, J. O., *Turbulence*, 2nd ed., McGraw-Hill, New York, 1975.
- 24 *ASHRAE Handbook of Fundamentals*, ASHRAE, New York, 1972.
- 25 "Thermal Performance Testing and Analysis of Photovoltaic Modules in Natural Sunlight," Jet Propulsion Laboratory, California Institute of Technology, Pasadena, CA, July 1977.
- 26 Scesa, S., and Sauer, F. M., "An Experimental Investigation of Convective Heat Transfer to Air from a Flat Plate with a Stepwise Discontinuous Surface Temperature," *Trans. ASME*, Vol. 74, 1952, pp. 1251-1255.
- 27 Sparrow, E. M., and Gregg, J. L., "Buoyancy Effects in Forced Convection Flow and Heat Transfer," *ASME J. Appl. Mech.*, Vol. 81E, 1959, pp. 133-134.

Effect of Flow Oscillations on Axial Energy Transport in a Porous Material

R. Siegel¹

Nomenclature

- A_s = internal surface area of porous medium per unit volume
- $C_1 \dots C_4$ = coefficients defined in equation (7)
- c_p = specific heat
- d_{\max} = maximum fluid displacement
- E_1, E_2 = coefficients in equation (13)
- F_1, F_2 = coefficients in equation (14)
- h = internal heat transfer coefficient
- K = constant of integration in equation (6)
- k = thermal conductivity (based on entire cross-sectional area)
- l = thickness of porous layer
- P = amplitude of oscillating pressure
- p = fluid pressure
- q = axial energy transport per unit cross-sectional area and time
- T = the part of t that depends only on time
- t = temperature
- u = Darcy velocity of fluid (volume flow/entire cross-sectional area)
- x = local coordinate across thickness of porous region
- $\alpha = C_1 h_m / \omega$
- γ = temperature gradient in x direction
- κ = permeability of porous material
- μ = fluid viscosity
- ρ = density
- τ = time

- ϕ = porosity of porous material (fluid volume/unit volume)
- ω = oscillation frequency

Subscripts

- a = amplitude of oscillating component
- C = cold reservoir
- f = fluid
- H = hot reservoir
- m = mean value
- P = particular solution
- s = solid

Introduction

It has been shown analytically and experimentally that flow oscillations of a fluid within a channel can enhance the axial transfer of energy. The transport arises from an axial gradient in fluid temperature resulting from having reservoirs at different temperatures at either end of the channel. A few recent references on enhanced axial transfer are given by [1-5], and these provide bibliography for earlier investigations.

The axial transport produced by fluid oscillations can be two or three orders of magnitude larger than molecular heat conduction. This augmentation is in the absence of throughflow in the channel. The amplitude of the flow oscillations is small compared with the channel length, so the enhancement is not produced by ordinary convective transport. As discussed in [3], the augmentation mechanism is involved with the transverse conduction between adjacent fluid layers moving relative to each other during the oscillations. The analyses in [1, 2] were for diffusion of a contaminant in oscillating laminar flow; since the channel walls were impervious, there was a zero normal derivative in contaminant concentration at the walls. The thermal energy equation has the same form as that for contaminant concentration; hence the analyses in [1, 2] could be extended for laminar energy diffusion in an insulated tube [4]. If the wall is not an insulator, energy can be exchanged with the wall during each oscillation. This transverse conduction enhances the energy transport in the axial direction, as shown in [5] for oscillating laminar flow in a channel with conducting walls.

The present analysis develops relations for axial energy diffusion in a porous medium with oscillating flow. In some devices, such as the Sterling engine, there are regenerators with oscillating flow. Axial transport in the regenerator provides an energy loss; hence it is desirable to determine what factors can limit this diffusion. A regenerator in the form of a porous medium is difficult to model since the flow is continually disrupted by the irregularities of the porous structure. The formulation here will employ an internal heat transfer coefficient that couples the fluid and solid temperatures. The final result shows how the diffusion depends on the magnitude of the heat transfer coefficient and the maximum fluid displacement. An assumption sometimes used in porous media heat transfer is that the good thermal conduct between fluid and solid within the small pores causes the fluid and solid to be at the same temperature locally. In this limit the induced axial diffusion becomes zero. Thus oscillation-induced losses may not be significant if the heat transfer ability within the porous structure is sufficiently high.

Analysis

The porous region is a plane layer of infinite extent in the y and z directions and of finite thickness from $x=0$ to l . A reservoir of hot fluid at T_H is adjacent to the face at $x=0$, and a reservoir of cold fluid at T_C is adjacent to $x=l$. There is no throughflow in the porous layer, but the fluid is oscillating in the x direction with an amplitude that is small compared with

¹NASA Lewis Research Center, Cleveland, OH 44135; Fellow ASME. Contributed by the Heat Transfer Division for publication in the JOURNAL OF HEAT TRANSFER. Manuscript received by the Heat Transfer Division October 24, 1985.